HHS Public Access

Author manuscript

Biol Psychiatry Cogn Neurosci Neuroimaging. Author manuscript; available in PMC 2017 September 29.

Published in final edited form as:

Biol Psychiatry Cogn Neurosci Neuroimaging. 2016 September ; 1(5): 448–459. doi:10.1016/j.bpsc.2016.06.008.

Reduced Neural Recruitment for Bayesian Adjustment of Inhibitory Control in Methamphetamine Dependence

Katia M. Harlé, **Shunan Zhang**, **Ning Ma**, **Angela J. Yu**, and **Martin P. Paulus**

Department of Psychiatry (KMH, MPP); and Department of Cognitive Science (SZ, NM, AJY), University of California, San Diego, La Jolla, California; and Laureate Institute for Brain Research (MPP), Tulsa, Oklahoma.

Abstract

Delineating the processes that contribute to the progression and maintenance of substance dependence is critical to understanding and preventing addiction. Several previous studies have shown inhibitory control deficits in individuals with stimulant use disorder. We used a Bayesian computational approach to examine potential neural deficiencies in the dynamic predictive processing underlying inhibitory function among recently abstinent methamphetamine-dependent individuals (MDIs), a population at high risk of relapse. Sixty-two MDIs were recruited from a 28-day inpatient treatment program at the San Diego Veterans Affairs Medical Center and compared with 34 healthy control subjects. They completed a stop-signal task during functional magnetic resonance imaging. A Bayesian ideal observer model was used to predict individuals' trial-to-trial probabilistic expectations of inhibitory response, P(stop), to identify group differences specific to Bayesian expectation and prediction error computation. Relative to control subjects, MDIs were more likely to make stop errors on difficult trials and had attenuated slowing following stop errors. MDIs further exhibited reduced sensitivity as measured by the neural tracking of a Bayesian measure of surprise (unsigned prediction error), which was evident across all trials in the left posterior caudate and orbitofrontal cortex (Brodmann area 11), and selectively on stop error trials in the right thalamus and inferior parietal lobule. MDIs are less sensitive to surprising task events, both across trials and upon making commission errors, which may help explain why these individuals may not engage in switching strategy when the environment changes, leading to adverse consequences.

Keywords

Addiction; Bayesian model; fMRI; Inhibitory control; Methamphetamine dependence; Prediction error

Amphetamine-type stimulants, which include methamphetamine, are the fastest rising drug of abuse worldwide and have become the second most widely used class of illicit drugs

Address correspondence to Katia M. Harlé, M.D., University of California San Diego, Laboratory of Biological Dynamics and Theoretical Medicine, Department of Psychiatry, 8939 Villa La Jolla Drive, Suite 200, La Jolla, CA, 92037-0985; kharle@ucsd.edu.

DISCLOSURES

The authors report no biomedical financial interests or potential conflicts of interest.

Supplementary material cited in this article is available online at http://dx.doi.org/10.1016/j.bpsc.2016.06.008.

worldwide (1,2). Moreover, methamphetamine dependence (MD) is associated with high likelihood of relapse (3). Whereas addiction research has heavily focused on reward processing, executive deficits have been consistently observed in stimulant abusers and implicated in the progression of abuse to dependence (4–6). Identifying precise neurocognitive processes of such deficits may therefore not only improve our understanding of how neurochemical changes in MD affect decision making, but also help identify robust neural predictors of relapse and treatment response.

Pharmacological, lesion, and neuroimaging studies suggest that neural alterations within the frontostriatal pathways, which appear to persist even during abstinence periods, may underlie the cognitive deficits observed in methamphetamine-dependent individuals (MDIs) (7–9). MDIs exhibit reduced integrity of dopaminergic and serotonergic neurons in dopamine-rich regions, including the anterior cingulate cortex (10,11), striatum (12), and limbic areas (13), and lower glucose metabolism in the striatum (14–16) and frontocingulate areas, including anterior cingulate, orbitofrontal, and dorsolateral prefrontal cortices (17–19). Such neural patterns have been linked to inhibitory and impulse-control deficits on standard interference/Stroop tasks (20,21) and in delay discounting (22–24). MDIs further show difficulties in detecting trends and integrating new information to predict future outcomes during decision making (25,26), which may be particularly hindering within changing environments, in which one has to constantly monitor information to know what to expect. Such learning impairment could contribute to MDIs' deficits in inhibitory control and other types of dynamic decision making (27). However, the cognitive processes underlying the relationship between neural damage and substance use in MDIs remain poorly understood.

In recent work, we showed that healthy individuals (28) and nondependent occasional stimulant users (29) continuously alter their response strategy in a standard inhibitory paradigm (stop-signal task), such that dynamic fluctuations in their reaction time and error rate are consistent with a particular Bayesian belief updating (30) and decision strategy (31). Here, we use the same Bayesian approach combined with event-related functional magnetic resonance imaging (fMRI) to model individuals' real-time expectations of response inhibition need in the stop-signal task. This strategy allows us to identify any difference between MDIs and healthy control subjects (CSs) in their neural representation of trialwise expectations of inhibitory response and Bayesian prediction errors needed for updating those expectations.

Based on the reduced functional metabolism in prefrontal, anterior cingulate, and striatal areas observed in MDIs, and given the consistent involvement of these brain regions in encoding action-related expectations, value, and prediction errors (29,32–34), we hypothesized that inhibitory dysfunction in MDIs would be characterized by attenuated neural representation of the expectation of an inhibitory signal, as well as altered prediction error signals, coding the discrepancy between predicted and actual outcomes, which is critical for adjusting expectations and adaptive behavior to potentially adverse consequences.

METHODS AND MATERIALS

Participants

The University of California, San Diego Human Research Protections Program approved the study protocol and all participants gave written informed consent. A total of 62 (21% female) recently abstinent (i.e., within the last month) MDIs were recruited from a 28-day inpatient Alcohol and Drug Treatment Program at the Veterans Affairs San Diego Health-care System and Scripps Green Hospital.[1] In addition, 34 healthy CSs (30% female) were recruited via flyers, internet ads (e.g., Craigslist), and local university newspapers. CSs were selected to be matched in age and IQ with MDIs. All subjects completed a clinical interview and a fMRI session during which they completed the stop-signal task (between the third and fourth week of treatment for MDIs). Lifetime DSM-IV Axes I and II diagnoses, including substance abuse and dependence (35), were assessed by the Semi-structured Assessment for the Genetics of Alcoholism II (SSAGA II) (36). Diagnoses were based on consensus meetings with a clinician specializing in substance use disorders (MPP) (see the Supplement for exclusion criteria).

Stop-Signal Task

Participants completed six blocks of a stop-signal task (75% go trials in each block) while undergoing fMRI. On go trials (n = 216, or 36/block), they had to press as quickly as possible the left button when an “X” appeared and the right button when an “O” appeared. On stop trials (i.e., whenever they heard a tone during a trial, at some time subsequent to the presentation of the go stimulus; n = 72), they were instructed not to press either button (see Figure 1A and Supplement for task instructions). Each trial lasted ≈1300 ms or until the participant responded, with a 200-ms interstimulus interval. Prior to scanning, participants’ mean go reaction time (i.e., average response latency [ARL]) from stimulus onset was determined to compute six levels of stop-signal delay (SSD), providing an individually customized range of difficulty [for more details see (29,37)].

Bayesian Model of Probabilistic Prediction

In recent work (28,31,38), sequential effects in the stop-signal paradigms, where recently experienced stop trials tend to increase reaction times (RTs) on a subsequent go trial and decrease error rate on a subsequent stop trial, have been shown to be well captured by a Bayes-optimal decision-making model. This Bayesian hidden Markov model adapted from the dynamic belief model (30) (see Figure 1B) assumes that an individual updates the previous probability of encountering stop trials, P(stop), on a trial-by-trial basis based on trial history and adjusts decision policy as a function of P(stop), with systematic consequences for go RT and stop accuracy in the upcoming trial. A higher predicted P(stop) is associated with a slower go RT and a higher likelihood of correctly stopping on a stop trial in healthy subjects (28,29). Briefly, the model assumes that the stop-signal frequency r_k on trial k has probability α of being the same as r_{k-1} and probability $1 - \alpha$ of being resampled from a previous βdistribution $p_0(r)$. The probability of trial k being a stop trial, P_k(stop) =

[1]To maintain sobriety during the program, participants were screened for the presence of drugs via urine toxicology.

$P(s_k{=}1 \mid \mathbf{S}_{k-1})$, where $\mathbf{S}_k = (s_1, \ldots, s_k)$ is 1 on stop trials and 0 on go trials, can be computed as follows:

$$\begin{aligned} P(s_k{=}1|\mathbf{S}_{k-1}) &= \int P(s_k{=}1|\mathrm{r}_k)\, p(\mathrm{r}_k|\mathbf{S}_{k-1})\, d\mathrm{r}_k \\ &= \int r_k p(r_k|\mathbf{S}_{k-1})\, dr_k = \langle r_k|\mathbf{S}_{k-1}\rangle \end{aligned}$$

The predictive probability of seeing a stop trial, $P_k(\text{stop})$, is the mean of the predictive distribution $p(r_k \mid \mathbf{s}_{k-1})$, which is a mixture of the previous posterior distribution and a fixed previous distribution, with α and 1–α acting as the mixing coefficients, respectively:

$$P(r_k|\mathbf{S}_{k-1}) = \alpha \mathrm{p}(r_{k-1}|\mathbf{S}_{k-1}) + (1-\alpha)\, p_0(r_k)$$

with the posterior distribution being updated according to Bayes's rule:

$$P(r_k|\mathbf{S}_k) \propto p(s_{k-1}|r_k)\, p(r_k|\mathbf{S}_{k-1})$$

Thus, to capture the persistent sequential effects, the model assumes that subjects continually update P(stop) with effectively the same learning rate, because they believe that the true rate of stop trials is undergoing changes in the environment: formally, with probability α, it stays the same as last trial, and with probability 1 – α, it is redrawn randomly from the generic previous distribution p_0. A larger α corresponds to a belief in a less volatile environment, and therefore a longer time window during which previous trials can affect future P(stop) calculations, which results in smaller sequential effects due to the most recently experienced go/stop trial (relative to a longer relevant time history) (30,38).

In the present study, parameters for the βdistribution $p_0(r)$ *and* α were kept constant across all subjects and were based on simulations that sought to optimize behavioral fit at the group level—that is, maximizing R^2 for the regression of P(stop) on RT. Such optimal parameters were p_0 = β(a = 2.5, b = 7.5; $s = a + b$ = 10; mean = 0.25) and α = 0.5. The fixed values were optimal for both groups.[2] Given these parameters and sequence of observed stop/go trials experienced by participants, we computed the corresponding sequence of subjective P(stop). In subsequent fMRI analyses, the trial-by-trial estimation of $P_k(\text{stop}) = P(s_k = 1 \mid \mathbf{S}_{k-1}) = \langle r_k \rangle$ (i.e., most up-to-date estimate of stop trial likelihood based on all previous trials) was used as a parametric regressor.

In previous work (30), we showed that the Bayesian belief updating model for P(stop) can be approximated by a linear-exponential filter of past observations, such that whether the previous trial was a stop trial (s_k = 1) or a go trial (s_k = 0) linearly contributes to the estimated P(stop) for the current trial, and the coefficient for each trial decays exponentially into the past. This model is also equivalent to a version of a delta rule, where P(stop) on each trial is an appropriately tuned linear combination of P(stop) on the last trial, how the most

[2]We specifically examined whether the model predictions would be sensitive to parameters α and the previous distribution $p_0(r)$ at the individual level (29) and found that produced P(stop) values were highly correlated across parameter settings and did not differ significantly between individual level or group level settings ($r > .9$; $R^2 > .8$). For this reason, we opted for fixed or universal parameter values across individuals.

recent observation (s_k = 1 or 0) differs from the last P(stop), in other words, a signed prediction error ($SPE_k = s_k – P_k$(stop)), and a constant bias term, which may be realistically implemented at the neural level (30).

Behavioral Statistical Analyses

We applied hierarchical generalized mixed-effect linear models to participants' trial accuracy (stop-success [SS] vs. stop-error [SE]) and RTs (dependent variables), treating subject as a random effect (with varying intercepts and slopes, unstructured variance/covariance assumed) and other independent variables as fixed effects (39). The first set of models for go RTs used a linear mixture of Bayesian model-based estimate of P(stop), group, previous trial type, and previous trial SSD. Go trials with a reaction time >1300 ms were automatically counted as go errors and were not included in those analyses. The second set of models for error data used a logit link function (40) in terms of linear mixtures of SSD, group, and P(stop). We report change in log-likelihood ratio (following a chi-squared distribution) and regression coefficients (when applicable) with associated *t* test and *p* values.

fMRI Analyses

Using a fast event-related fMRI design, six T2*-weighted echo planar imaging functional runs were collected for each participant, along with one T1-weighted anatomical image (see the Supplement for image acquisition and preprocessing details). Preprocessing and subsequent fMRI analyses were conducted using Analysis of Functional NeuroImages (AFNI) software (41).

First-Level Analyses—Three types of trials were distinguished (go, SS, and SE; go error trials were scarce and not included in these analyses), included as predictors in a general linear model (GLM), and convolved with a canonical hemodynamic response function. They were entered as linear regressors (multiplied by the mean of the computed P(stop) probabilities across all trials) and were parametrically modulated by P(stop) (29,42) in order to isolate neural activations associated with P(stop) independently of categorical trial type neural coding (i.e., categorical regressors). This model therefore included six task regressors (three categorical: go, SS, SE; and three model-based parametric: GoxP_k(stop), SSxP_k(stop), SExP_k(stop)). To assess group differences in the updating processes related to P(stop), we created a second GLM with trialwise Bayesian signed prediction error [i.e., SPE: (outcome-P(stop)] and unsigned prediction error [i.e., UPE: |outcome-P(stop)|] as parametric regressors of interest. This second model also included a parametric regressor modeling trial error (0 = correct or 1 = error) to control for performance error-related activity (28). Given the fixed parameter setting and pseudorandomized sequence of trials, the P(stop) and Bayesian UPE/SPE values were the same for all participants in these GLMs. Both GLMs included a baseline regressor (consisting of intertrial intervals), instruction phases, linear drift, and three motion regressors [pitch, yaw, roll (37)], go RTs, and SSD as parametric regressors of no interest (see the Supplement for regressor correlations). Images were spatially filtered (Gaussian full width half maximum 4 mm) to account for individual anatomical differences. Anatomical and functional images were manually transformed into Talairach space.

Second-Level Analyses—At the between-subject level, the coefficients of our first-level GLM were modeled with voxel-wise mixed-effects linear models analyses, performed with R statistical software (R Foundation for Statistical Computing, Vienna, Austria) (43), in terms of a linear mixture of subject-level effects and group (CS, MDI). Specifically, we tested for second-level effects of group and its interaction with P(stop) under each trial type ($GoxP_k$(stop), $SSxP_k$(stop), $SExP_k$(stop)), with subject treated as a random effect.[3] In the first analysis, we isolated P(stop)-modulated activations for go versus stop trials (SS and SE were averaged). Whole brain statistical maps were obtained for the group main effect (reflecting areas tracking previous P(stop) values irrespective of trial type or accuracy) and the groupxP(stop) modulated trial type interaction. We then conducted an additional contrast on stop trials only, comparing P(stop) modulated activation for SS versus SE trials and obtained statistical maps for the groupxP (stop) trial type (SE vs. SS) interaction. To correct for multiple comparisons, we used a cluster threshold adjustment based on Monte Carlo simulations (generated with AFNI's 3dClust-Sim program), based on whole-brain voxel size and 4-mm smoothness. A minimum cluster volume of 768 μL was used, with a minimum voxelwise significance of $p < .005$, corrected for multiple comparisons at familywise error rate = $p < .01$.

Group Difference in Bayesian Prediction Errors—Based on previous work (28,29), we further selected from areas identified in the interaction contrast of the above-mentioned analyses [interaction of group and P(stop)-modulated trial type, i.e., GoxP(stop), StopxP(stop)] those that were consistent with a group difference in either type of Bayesian prediction errors (UPE and SPE). Specifically, we identified those regions with nonzero P(stop) activations in CSs of opposite signs and same signs across go and stop trials, reflecting UPE and SPE activations respectively (see the Supplement).

RESULTS

Subject Characteristics

MDI did not differ from CS in ethnicity, sex, age, and verbal IQ ($p > .05$). On average, CSs had a higher level of education ($p < .001$). MDIs endorsed greater cocaine and cannabis intake ($p < .001$), and they used alcohol and nicotine more frequently and in larger quantities than did CSs ($p < .05$) (see Table 1 and the Supplement).

Behavioral Performance and Model-Based Behavioral Adjustment

Reaction Times—Consistent with our model's assumptions (28,31,38), a positive linear relationship between go RT and P(stop) was observed across both groups ($B = 274$ ms, $t(94) = 4.6$, $p < .001$, model omnibus test: $\chi^2(1) = 19.4$, $p < .001$; mean Pearson Correlation Coefficient: $r = .15$, adjusted $R^2 = .05$). The group main effect on go RT was not statistically significant ($\chi^2(1) = 0.48$, $p = .49$); mean RT: CS = 624 ms; MDI = 590 ms) (see Figure 2A for go RT distributions). By P(stop) interaction, the group was marginally significant ($\chi^2(1) = 3.8$, $p = .05$), showing a trend for smaller positive slope for RT as a function of P(stop) in

[3]Reported lifetime uses of marijuana and typical numbers of alcoholic drinks and cigarettes per day were included as covariates in the longitudinal mixed effects analysis to control for the effect of nonstimulant drug use.

CSs. Whereas the regression slope was steeper in MDIs, we surmise that this pattern relates to the wider RT range (more short RTs) and the larger sample size in MDIs, rather than reflecting a meaningful group difference in model fit and related neural processes. A positive linear relationship between go RT and P(stop) was observed within each group (CS: B = 105, $p < .01$; $\chi^2(1) = 7.7$, $p < .01$; MDI: $B = 365$, $p < .001$; $\chi^2(1) = 144$, $p < .001$). For illustration of the linear trends, Figure 2B shows data collapsed across all subjects for MDIs and CSs separately, where go trials were binned by P(stop) and average RT calculated for each bin separately. MDIs and CSs did not differ in stop signal reaction time (mean CS = 239 ms; mean MDI = 231 ms, $t(94) = .49$, p = .61) (see the Supplement for stop signal reaction time computation).

Poststop Slowing—An overall slowing in go RT was observed following stop relative to go trials ($\chi^2(1) = 124$, $p < .001$), which was true for both SS ($B = +17$, $p < .001$) and SE ($B = +35$, $p < .001$) trials. Moreover, there was a group by previous trial type interaction ($\chi^2(1) = 41$, $p < .001$). Specifically, CSs had similar RTs following SS and go trials ($B = 6$, $t(33) = -1.3$, $p = .18$) but exhibited significant slowing following SE trials ($B = 16$, $t(32) = 2.9$, $p < .01$). In contrast, MDIs were overall slower following SS relative to go trials ($B = 31$, $t(62) = 5.4$, $p < .001$) but did not exhibit additional slowing after SE relative to SS trials ($B = 10$, $t(62) = -1.5$, $p = .19$) (see Figure 2C and the Supplement).

Performance Accuracy—As expected, participants had a higher likelihood of error on trials with longer SSD (odds ratio = 2.6, Wald $z = 39$, $p < .001$; omnibus test: $\chi^2(1) = 250$, $p < .001$). The group difference in stop error rates did not reach statistical significance (group main effect: $\chi^2(1) = 2.3$, $p = .13$; mean error rates: CS = 0.44; MDI = 0.49); however, the group by SSD interaction was significant ($\chi^2(1) = 4.8$, $p < .05$) with higher error likelihood in MDI for longer SSD (i.e., more difficult SSD) (see Figure 2D). Moreover, as predicted by our model (28,31,38), we found a negative relationship between error likelihood and P(stop), with higher P(stop) overall prompting a smaller likelihood of error (odds ratio = 0.10, Wald $z = -3.38$, $p < .001$; omnibus test: $\chi^2(1) = 11.4$, $p < .001$). Other interactions (i.e., P(Stop)xGroup, P(stop)xSSD, P(stop)xSSDxGroup) did not reach statistical significance ($p > .05$).

fMRI Analyses

Bayesian Prediction of Inhibitory Response (P(Stop))—Testing for any group differences in brain activation associated with P(stop), after regressing out any variance correlated with actual stimulus outcome (stop vs. go), we found no areas consistent with such neural pattern.

Modulation of Bayesian Prediction of Inhibitory Response (P(Stop)) by Trial Type (Stop vs. Go)—Seven regions were associated with a significant interaction between groups (CS vs. MDI) and P(stop)-modulated trial type [StopxP (stop) vs. GoxP(stop)]. These regions and their coordinates are listed in Table 2. In five of those regions (right hemisphere regions and left caudate), MDIs showed a positive activation associated with P(stop) on stop trials ($p < .05$), but no significant P(stop) activation on go trials ($p > .05$). CSs showed no significant P(stop) activations to go or stop trials in these regions ($p > .05$).

In the other two regions (left posterior caudate and orbitofrontal cortex [OFC]/Brodmann area 11 [BA 11]) (see Figures 3A and 4A), CSs showed a negative correlation with P(stop) on stop trials and positive correlation with P(stop) on go trials, consistent with a positive UPE (UPE = |outcome-P(stop)|) (see Supplement). However, unlike CSs, MDIs failed to show a differential P(stop) activation to go versus stop trials in those regions (see Figures 3B and 4B). Importantly, based on supplemental analyses, CSs showed activation positively correlated with a UPE in these areas, whereas MDIs had significantly attenuated UPE activations, which was not statistically different from zero (Cohen's $d = .45$ and .42 for left posterior caudate and OFC/BA 11, respectively) (see Figure 3C and 4C).

Modulation of Bayesian Prediction of Inhibitory Response (P(Stop)) by Stop Accuracy (SS vs. SE)—Activation in several neural regions were associated with a significant interaction between group and P(stop) modulated stop accuracy (SS vs. SE trials) (see Table 3 for coordinates). In all regions, CSs exhibited a significant negative correlation to P(stop) on SE trials and a positive correlation to P(stop) on SS trials ($p < .05$), whereas MDI showed no significant P(stop) activation on either SS or SE trials ($p > .05$).

To further assess whether these activation patterns may be linked to group difference in the coding of Bayesian predication errors, we extracted activation associated with both UPE and SPE in those five regions. Only two of these areas (right thalamus and right inferior parietal lobule [IPL]/BA 40) (see Figures 5A and 6A) were associated with activation patterns consistent with a selective encoding of a positive UPE on SE trials among CSs. In contrast, MDIs showed no significant activations to UPE on SE or any other trials (Cohen's $d = .41$ and .62 in right thalamus and IPL, respectively) (see Figures 5B–C and 6B–C). Correlational analyses further showed that such UPE activation on SE trials among CSs (not significantly different from zero in MDIs) was associated with lower error rates for difficult trials ($r = -.47$, $p < .05$) (see Figure 6D).

DISCUSSION

The goal of this investigation was to better delineate which processes are dysfunctional in a group of recently abstinent MDIs. We applied a Bayesian model to evaluate the probability of a stop signal and used this probability to quantify the degree of neural processing of “the need to stop,” and of the discrepancy between observations and actual outcomes—that is, sensitivity to surprising outcomes—based on associated prediction errors. MDIs exhibited a pattern of reduced neural activation associated with trial-level Bayesian prediction error signals (i.e., more surprise) in orbitofrontal frontal, parietal, and subcortical areas (caudate and thalamus). Consistent with evidence of impaired inhibitory function in this population (20,21,44), MDIs compared with CSs were less accurate during more difficult trials (i.e., longer SSD). In addition, MDIs did not show evidence of strategic adjustment after a stop error; in other words, they did not show response time slowing after an error. Nevertheless, both CSs and MDIs maintain and use an internal representation of stop trial probability to make anticipatory adjustments for inhibitory control (e.g., in their reaction times) based on trial history, which supports our modeling approach and is consistent with previous work (28,29).

Relative to CSs, MDIs had attenuated neural activation associated with a Bayesian model-based UPE in the left OFC and posterior caudate. Whereas both the OFC and caudate have been implicated in stimulus-reward learning and value-based decision making (45,46), these areas are also critical for prediction and processing of performance feedback during decision making (26,47,48), including signaling expectation violation (49) and prediction errors (34,50–53). Importantly, failure to recruit the OFC has been linked to impulsivity and poor inhibitory function (54), as well as to impaired learning of stimulus-outcome contingencies in MDIs (26). A group difference in unsigned Bayesian prediction error, as opposed to an action-dependent SPE or nonmodel-based error activity, may further suggest specific deficits among MDIs in tracking the overall inconsistency between environmental demands and their internal belief/prediction model (i.e., a “goodness-of-fit” estimate), rather than action-specific inconsistency, with negative consequences on inhibitory performance. Thus, rather than promoting a failure to recruit specific frontostriatal regions to predict appropriate actions, MD may impair neural tracking of model-based expectancy violation, which may be useful more generally in preparing individuals for switching strategy in response to significant changes in the environment (30,55) (e.g., sudden change in reward rate), rather than in model updating (i.e., P(stop) estimation). The absence of group difference in overall p (stop) activations across trial type indeed suggests that groups did not differ in their mean estimates of P(stop), which lends credence to this interpretation.

Interestingly, MDIs further exhibited poorer neural encoding of stopping expectations [i.e., P(stop)] on SE trials in a set of parietal and subcortical regions, consistent with their failure to slow down following SE trials. Specifically, CSs but not MDIs activated the right thalamus and IPL proportionally to a positive UPE on SE trials relative to other trials (go and SS). Such UPE activations were associated with lower error rates for difficult trials among CSs, suggesting that this selective UPE encoding (attenuated or absent in MDIs) may be particularly important to adjust and improve inhibitory performance. Such results are congruent with evidence of prediction error signaling in the thalamus (56,57) and the IPL, with functional connections to the dorsal caudate (58) and premotor areas (59), which has also been implicated in predictive coding (60,61), and most recently in instrumental (action-reward) contingency learning (62) and tracking the degree of divergence/volatility in instrumental action probability distributions (63).

This study has several limitations. First, we recognize that our computations of prediction errors are not inherently Bayesian, and they overlap with Bayesian and Information Theory estimates of precision, volatility (64), and surprise (65). Brain processes associated with UPE/SPE are, however, an important first step and provide good approximations of the optimal Bayesian model updating (30,55). Nevertheless, the present study did not explicitly measure volatility and model accuracy or precision, and thus cannot address whether the observed neural difference in UPE may reflect a difference in Bayesian estimates of volatility (i.e., degree of expectancy violation) or in precision (inversely related to the variance around mean expectation). Second, our model could be refined by including a more direct prediction of behavior such as RTs, as we have done behaviorally in previous work (31). Such approach, however, would require significantly larger data collection owing to additional model parameters, which was not feasible for this fMRI study. Finally, we note that participants’ interpretation of the SST instructions, which include incentives to limit

poststop error slowing, may lend some level of confound in the interpretation of our results, for example, reduced poststop slowing could relate to more rigid instructions following in MDIs.

In summary, the present findings suggest that both cortical and subcortical structures in MDIs fail to adequately track the changes in environmental characteristics that would help to predict the need for increased inhibition. Importantly, using the same parameter values across groups allowed us to assess group differences in an objective measure of the "need to stop" and the "surprise" associated with each trial (i.e., participant's sensitivity to surprising or informative trials) in terms of their behavioral and neuronal responses. Our results further suggest this group difference may reflect MDIs' poorer tracking of expectancy violation (i.e., weaker sensitivity to surprising task events), rather than real-time mean predictions per se. Although we did observe a relationship between UPE activations in the IPL and error rates, suggesting a negative impact of such weaker activations in MDIs on their behavioral performance, future studies are needed to determine how such neural alterations may specifically relate to Bayesian estimates of volatility and precision, and how they may directly impact performance. This study highlights the utility of Bayesian learning models for investigating subtle cognitive alterations guiding goal-directed actions in addiction and other psychiatric populations, which can be used to develop precise addiction medicine approaches for better diagnosis and treatment of this disorder.

Supplementary Material

Refer to Web version on PubMed Central for supplementary material.

ACKNOWLEDGMENTS

This work was supported by grants from the National Institute on Drug Abuse (R01-DA016663, P20-DA027834, R01-DA027797, and R01-DA018307, as well as a Veterans Affairs Merit Grant to MPP).

REFERENCES

1. Degenhardt L, Mathers B, Guarinieri M, Panda S, Phillips B, Strathdee SA, et al. for Reference Group to the United Nations on HIV and Injecting Drug Use. Meth/amphetamine use and associated HIV: Implications for global policy and public health. Int J Drug Policy. 2010; 21:347–358. [PubMed: 20117923]
2. Panenka WJ, Procyshyn RM, Lecomte T, MacEwan GW, Flynn SW, Honer WG, Barr AM. Methamphetamine use: A comprehensive review of molecular, preclinical and clinical findings. Drug Alcohol Depend. 2013; 129:167–179. [PubMed: 23273775]
3. Brecht ML, Herbeck D. Time to relapse following treatment for methamphetamine use: A long-term perspective on patterns and predictors. Drug Alcohol Depend. 2014; 139:18–25. [PubMed: 24685563]
4. Gowin JL, Harlé KM, Stewart JL, Wittmann M, Tapert SF, Paulus MP. Attenuated insular processing during risk predicts relapse in early abstinent methamphetamine-dependent individuals. Neuropsychopharmacology. 2014; 39:1379–1387. [PubMed: 24317375]
5. Clark VP, Beatty GK, Anderson RE, Kodituwakku P, Phillips JP, Lane TDR, et al. Reduced fMRI activity predicts relapse in patients recovering from stimulant dependence. Human Brain Mapp. 2012; 35:414–428.

6. Paulus MP, Tapert SF, Schuckit MA. Neural activation patterns of methamphetamine-dependent subjects during decision making predict relapse. Arch Gen Psychiatry. 2005; 62:761–768. [PubMed: 15997017]
7. Baicy K, London ED. Corticolimbic dysregulation and chronic methamphetamine abuse. Addiction. 2007; 102(suppl 1):5–15.
8. Fillmore MT. Drug abuse as a problem of impaired control: current approaches and findings. Behav and Cogn Neurosci Rev. 2003; 2:179–197. [PubMed: 15006292]
9. Jentsch JD, Taylor JR. Impulsivity resulting from frontostriatal dysfunction in drug abuse: implications for the control of behavior by reward-related stimuli. Psychopharmacology (Berl). 1999; 146:373–390. [PubMed: 10550488]
10. Nordahl TE, Salo R, Natsuaki Y, Galloway GP, Waters C, Moore CD, et al. Methamphetamine users in sustained abstinence: A proton magnetic resonance spectroscopy study. Arch Gen Psychiatry. 2005; 62:444–452. [PubMed: 15809412]
11. Salo R, Nordahl TE, Natsuaki Y, Leamon MH, Galloway GP, Waters C, et al. Attentional control and brain metabolite levels in methamphetamine abusers. Biol Psychiatry. 2007; 61:1272–1280. [PubMed: 17097074]
12. Chang L, Alicata D, Ernst T, Volkow N. Structural and metabolic brain changes in the striatum associated with methamphetamine abuse. Addiction. 2007; 102:16–32. [PubMed: 17493050]
13. Thompson PM, Hayashi KM, Simon SL, Geaga JA, Hong MS, Sui Y, et al. Structural abnormalities in the brains of human subjects who use methamphetamine. J Neurosci. 2004; 24:6028–6036. [PubMed: 15229250]
14. Sekine Y, Minabe Y, Kawai M, Suzuki K, Iyo M, Isoda H, et al. Metabolite alterations in basal ganglia associated with methamphetamine-related psychiatric symptoms: A proton MRS study. Neuropsychopharmacology. 2002; 27:453–461. [PubMed: 12225702]
15. Volkow ND, Chang L, Wang GJ, Fowler JS, Franceschi D, Sedler MJ, et al. Higher cortical and lower subcortical metabolism in detoxified methamphetamine abusers. Am J Psychiatry. 2001; 158:383–389. [PubMed: 11229978]
16. Nestor LJ, Ghahremani DG, Monterosso J, London ED. Prefrontal hypoactivation during cognitive control in early abstinent methamphetamine-dependent subjects. Psychiatry Res. 2011; 194:287–295. [PubMed: 22047731]
17. Sekine Y, Minabe Y, Ouchi Y, Takei N, Iyo M, Nakamura K, et al. Association of dopamine transporter loss in the orbitofrontal and dorsolateral prefrontal cortices with methamphetamine-related psychiatric symptoms. Am J Psychiatry. 2003; 160:1699–1701. [PubMed: 12944350]
18. Kim YT, Lee SW, Kwon DH, Seo JH, Ahn BC, Lee J. Dose-dependent frontal hypometabolism on FDG-PET in methamphetamine abusers. J Psychiatr Res. 2009; 43:1166–1170. [PubMed: 19394959]
19. London ED, Simon SL, Berman SM, Mandelkern MA, Lichtman AM, Bramen J, et al. Mood disturbances and regional cerebral metabolic abnormalities in recently abstinent methamphetamine abusers. Arch Gen Psychiatry. 2004; 61:73–84. [PubMed: 14706946]
20. Simon SL, Dean AC, Cordova X, Monterosso JR, London ED. Methamphetamine dependence and neuropsychological functioning: Evaluating change during early abstinence. J Stud Alcohol Drugs. 2010; 71:335–344. [PubMed: 20409426]
21. Tabibnia G, Monterosso JR, Baicy K, Aron AR, Poldrack RA, Chakrapani S, et al. Different forms of self-control share a neurocognitive substrate. J Neurosci. 2011; 31:4805–4810. [PubMed: 21451018]
22. Hoffman WF, Moore M, Templin R, McFarland B, Hitzemann RJ, Mitchell SH. Neuropsychological function and delay discounting in methamphetamine-dependent individuals. Psychopharmacology (Berl). 2006; 188:162–170. [PubMed: 16915378]
23. Kirby KN, Petry NM. Heroin and cocaine abusers have higher discount rates for delayed rewards than alcoholics or non-drug-using controls. Addiction. 2004; 99:461–471. [PubMed: 15049746]
24. Wittmann M, Leland DS, Churan J, Paulus MP. Impaired time perception and motor timing in stimulant-dependent subjects. Drug Alcohol Depend. 2007; 90:183–192. [PubMed: 17434690]
25. Rogers RD, Everitt B, Baldacchino A, Blackshaw A, Swainson R, Wynne K, et al. Dissociable deficits in the decision-making cognition of chronic amphetamine abusers, opiate abusers, patients

with focal damage to prefrontal cortex, and tryptophan-depleted normal volunteers: Evidence for monoaminergic mechanisms. Neuropsychopharmacology. 1999; 20:322–339. [PubMed: 10088133]

26. Paulus MP, Hozack NE, Zauscher BE, Frank L, Brown GG, Braff DL, Schuckit MA. Behavioral and functional neuroimaging evidence for prefrontal dysfunction in methamphetamine-dependent subjects. Neuropsychopharmacology. 2002; 26:53–63. [PubMed: 11751032]
27. Aron JL, Paulus MP. Location, location: Using functional magnetic resonance imaging to pinpoint brain differences relevant to stimulant use. Addiction. 2007; 102(suppl 1):33–43. [PubMed: 17493051]
28. Ide JS, Shenoy P, Yu AJ, Li CS. Bayesian prediction and evaluation in the anterior cingulate cortex. J Neurosci. 2013; 33:2039–2047. [PubMed: 23365241]
29. Harlé KM, Shenoy P, Stewart JL, Tapert SF, Angela JY, Paulus MP. Altered neural processing of the need to stop in young adults at risk for stimulant dependence. J Neurosci. 2014; 34:4567–4580. [PubMed: 24672002]
30. Yu AJ, Cohen JD. Sequential effects: Superstition or rational behavior. Adv Neural Inf Process Syst. 2008; 21:1873–1880. [PubMed: 26412953]
31. Shenoy P, Angela JY. Rational decision-making in inhibitory control. Front Hum Neurosci. 2011; 5:48. [PubMed: 21647306]
32. Kennerley SW, Behrens TE, Wallis JD. Double dissociation of value computations in orbitofrontal and anterior cingulate neurons. Nature Neurosci. 2011; 14:1581–1589. [PubMed: 22037498]
33. Somerville LH, Heatherton TF, Kelley WM. Anterior cingulate cortex responds differentially to expectancy violation and social rejection. Nat Neurosci. 2006; 9:1007–1008. [PubMed: 16819523]
34. Menon M, Jensen J, Vitcu I, Graff-Guerrero A, Crawley A, Smith MA, Kapur S. Temporal difference modeling of the blood-oxygen level dependent response during aversive conditioning in humans: Effects of dopaminergic modulation. Biol Psychiatry. 2007; 62:765–772. [PubMed: 17224134]
35. APA. Diagnostic and Statistical Manual of Mental Disorders. 5th ed.. American Psychiatric Publishing; Washington, DC: 2013.
36. Bucholz KK, Cadoret R, Cloninger CR, Dinwiddie SH, Hesselbrock VM, Nurnberger JI Jr, et al. A new, semi-structured psychiatric interview for use in genetic linkage studies: A report on the reliability of the SSAGA. J Stud Alcohol. 1994; 55:149–158. [PubMed: 8189735]
37. Matthews SC, Simmons AN, Arce E, Paulus MP. Dissociation of inhibition from error processing using a parametric inhibitory task during functional magnetic resonance imaging. Neuroreport. 2005; 16:755–760. [PubMed: 15858420]
38. Shenoy P, Rao RPN, Yu A. A rational decision making framework for inhibitory control. Adv Neural Inf Process Syst 24. 2011
39. Baayen RH, Davidson DJ, Bates DM. Mixed-effects modeling with crossed random effects for subjects and items. J Mem Lang. 2008; 59:390–412.
40. Jaeger TF. Categorical data analysis: Away from ANOVAs (transformation or not) and towards logit mixed models. J Mem Lang. 2008; 59:434–446. [PubMed: 19884961]
41. Cox RW. AFNI: Software for analysis and visualization of functional magnetic resonance neuroimages. Comput Biomed Res. 1996; 29:162–173. [PubMed: 8812068]
42. Büchel C, Holmes AP, Rees G, Friston KJ. Characterizing stimulus-response functions using nonlinear regressors in parametric fMRI experiments. Neuroimage. 1998; 8:140–148. [PubMed: 9740757]
43. Pinheiro, J., Bates, D., DebRoy, S., Sarkar, D. R package version 3.1-102. R Foundation for Statistical Computing; Vienna, Austria: 2011. The R Development Core Team 2011 nlme: Linear and nonlinear mixed effects models.. Available at: http://cranr-projectorg/web/packages/nlme/index.html. Accessed
44. Monterosso JR, Aron AR, Cordova X, Xu J, London ED. Deficits in response inhibition associated with chronic methamphetamine abuse. Drug Alcohol Depend. 2005; 79:273–277. [PubMed: 15967595]
45. Wallis JD. Orbitofrontal cortex and its contribution to decision-making. Annu Rev Neurosci. 2007; 30:31–56. [PubMed: 17417936]

46. O'Doherty JP. Reward representations and reward-related learning in the human brain: Insights from neuroimaging. Curr Opin Neurobiol. 2004; 14:769–776. [PubMed: 15582382]
47. Elliott R, Frith CD, Dolan RJ. Differential neural response to positive and negative feedback in planning and guessing tasks. Neuropsychologia. 1997; 35:1395–1404. [PubMed: 9347486]
48. Elliott R, Rees G, Dolan RJ. Ventromedial prefrontal cortex mediates guessing. Neuropsychologia. 1999; 37:403–411. [PubMed: 10215087]
49. Nobre AC, Coull JT, Frith CD, Mesulam MM. Orbitofrontal cortex is activated during breaches of expectation in tasks of visual attention. Nat Neurosci. 1999; 2:11–12. [PubMed: 10195173]
50. Ramnani N, Elliott R, Athwal BS, Passingham RE. Prediction error for free monetary reward in the human prefrontal cortex. Neuro-image. 2004; 23:777–786. [PubMed: 15528079]
51. Delgado MR, Li J, Schiller D, Phelps EA. The role of the striatum in aversive learning and aversive prediction errors. Philos Trans R Soc Lond B: Biol Sci. 2008; 363:3787–3800. [PubMed: 18829426]
52. Haruno M, Kawato M. Different neural correlates of reward expectation and reward expectation error in the putamen and caudate nucleus during stimulus-action-reward association learning. J Neurophysiol. 2006; 95:948–959. [PubMed: 16192338]
53. Mattfeld AT, Gluck MA, Stark CE. Functional specialization within the striatum along both the dorsal/ventral and anterior/posterior axes during associative learning via reward and punishment. Learn Mem. 2011; 18:703–711. [PubMed: 22021252]
54. Horn NR, Dolan M, Elliott R, Deakin JF, Woodruff PW. Response inhibition and impulsivity: An fMRI study. Neuropsychologia. 2003; 41:1959–1966. [PubMed: 14572528]
55. Tervo DG, Proskurin M, Manakov M, Kabra M, Vollmer A, Branson K, Karpova AY. Behavioral variability through stochastic choice and its gating by anterior cingulate cortex. Cell. 2014; 159:21–32. [PubMed: 25259917]
56. Ploghaus A, Tracey I, Clare S, Gati JS, Rawlins JN, Matthews PM. Learning about pain: The neural substrate of the prediction error for aversive events. Proc Natl Acad Sci U S A. 2000; 97:9281–9286. [PubMed: 10908676]
57. Kim H, Shimojo S, O'Doherty JP. Is avoiding an aversive outcome rewarding? Neural substrates of avoidance learning in the human brain. PLoS Biol. 2006; 4:e233. [PubMed: 16802856]
58. Di Martino A, Scheres A, Margulies D, Kelly AM, Uddin LQ, Shehzad Z, et al. Functional connectivity of human striatum: A resting state FMRI study. Cereb Cortex. 2008; 18:2735–2747. [PubMed: 18400794]
59. Rushworth MF, Behrens TE, Johansen-Berg H. Connection patterns distinguish 3 regions of human parietal cortex. Cereb Cortex. 2006; 16:1418–1430. [PubMed: 16306320]
60. Knutson B, Wimmer GE. Splitting the difference: How does the brain code reward episodes? Ann N Y Acad Sci. 2007; 1104:54–69. [PubMed: 17416922]
61. Spoormaker VI, Andrade KC, Schröter MS, Sturm A, Goya-Maldonado R, Sämann PG, Czisch M. The neural correlates of negative prediction error signaling in human fear conditioning. Neuroimage. 2011; 54:2250–2256. [PubMed: 20869454]
62. Liljeholm M, Tricomi E, O'Doherty JP, Balleine BW. Neural correlates of instrumental contingency learning: Differential effects of action-reward conjunction and disjunction. J Neurosci. 2011; 31:2474–2480. [PubMed: 21325514]
63. Liljeholm M, Wang S, Zhang J, O'Doherty JP. Neural correlates of the divergence of instrumental probability distributions. J Neurosci. 2013; 33:12519–12527. [PubMed: 23884955]
64. Behrens TE, Woolrich MW, Walton ME, Rushworth MF. Learning the value of information in an uncertain world. Nat Neurosci. 2007; 10:1214–1221. [PubMed: 17676057]
65. Mars RB, Debener S, Gladwin TE, Harrison LM, Haggard P, Rothwell JC, Bestmann S. Trial-by-trial fluctuations in the event-related electroencephalogram reflect dynamic changes in the degree of surprise. J Neurosci. 2008; 28:12539–12545. [PubMed: 19020046]

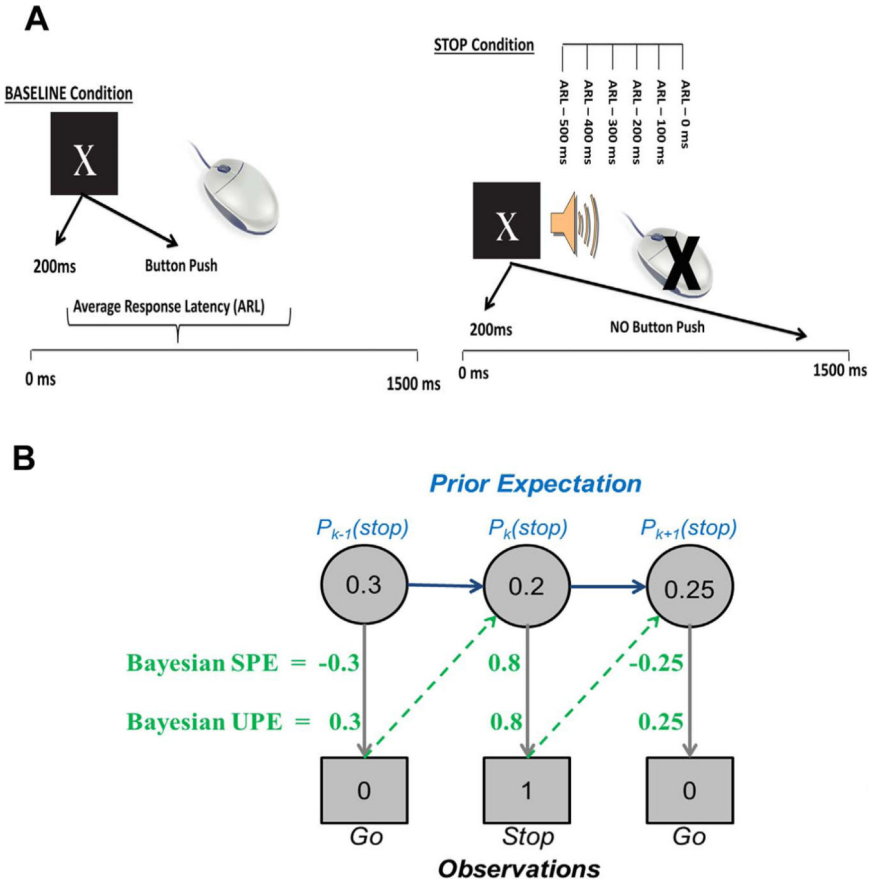

Figure 1.

(A) Stop signal task. Participants completed a total of 288 trials, including 216 go trials (baseline condition), and 72 stop trials. Each trial lasted 1300 ms and trials were separated by 200-ms interstimulus intervals (blank screen). Participants performed six blocks of 48 trials (25% stop and 75% go trials in each block). Trial order was pseudo-randomized throughout the task and counterbalanced. Prior to scanning, participants performed the stop task outside the scanner in order to determine their average response latency ([ARL]; i.e., mean reaction time on go trials). Such individual measures were used to determine the stop signal delay for the six different stop trial types, providing a subject-dependent jittered reference function. Specifically, stop signals were delivered at 0 (ARL-0), 100 (ARL-100), 200 (ARL-200), 300 (ARL-300), 400 (ARL-400), or 500 (ARL-500) ms less than the mean reaction time after the beginning of the trial, thus providing a range of difficulty level; ARL ranged from 504 to 925 ms (mean = 664 ms, SD = 112 ms). Task instructions: Participants were instructed to “press as quickly as possible the left button when an ‘X’ appears, or the right button when an ‘O’ appears.” They were also instructed not to press either button whenever they heard a tone during a trial (stop condition). **(B)** Bayesian hidden Markov model used, a version of the dynamic belief model (30), which computes trialwise sequential predictions about the frequency of stop trials. The model assumes that subjects constantly anticipate the likelihood of encountering stop trials, P(stop), on a trial-by-trial basis based on trial history, whereby experienced stop trials increase P(stop) and go trials decrease P(stop). A change in P(stop) then changes the decision strategy within a trial, such that the overall

objective function, encompassing costs related to response delay, stop errors, and go errors, is optimized by an ideal observer who, faced with a larger P(stop), reduces stop error costs by lowering stop error rate and increasing go reaction time. The previous probability of encountering a stop signal on trial k, P_k(stop), is compared with the actual trial outcome (0 = go; 1 = stop) to produce a signed prediction error ([SPE]; i.e., outcome-P_k(stop)), which is combined with the prior to produce a new updated prior for the next trial $k + 1$ (see the Supplement). UPE, unsigned prediction error (i.e., |outcome-P(stop)|).

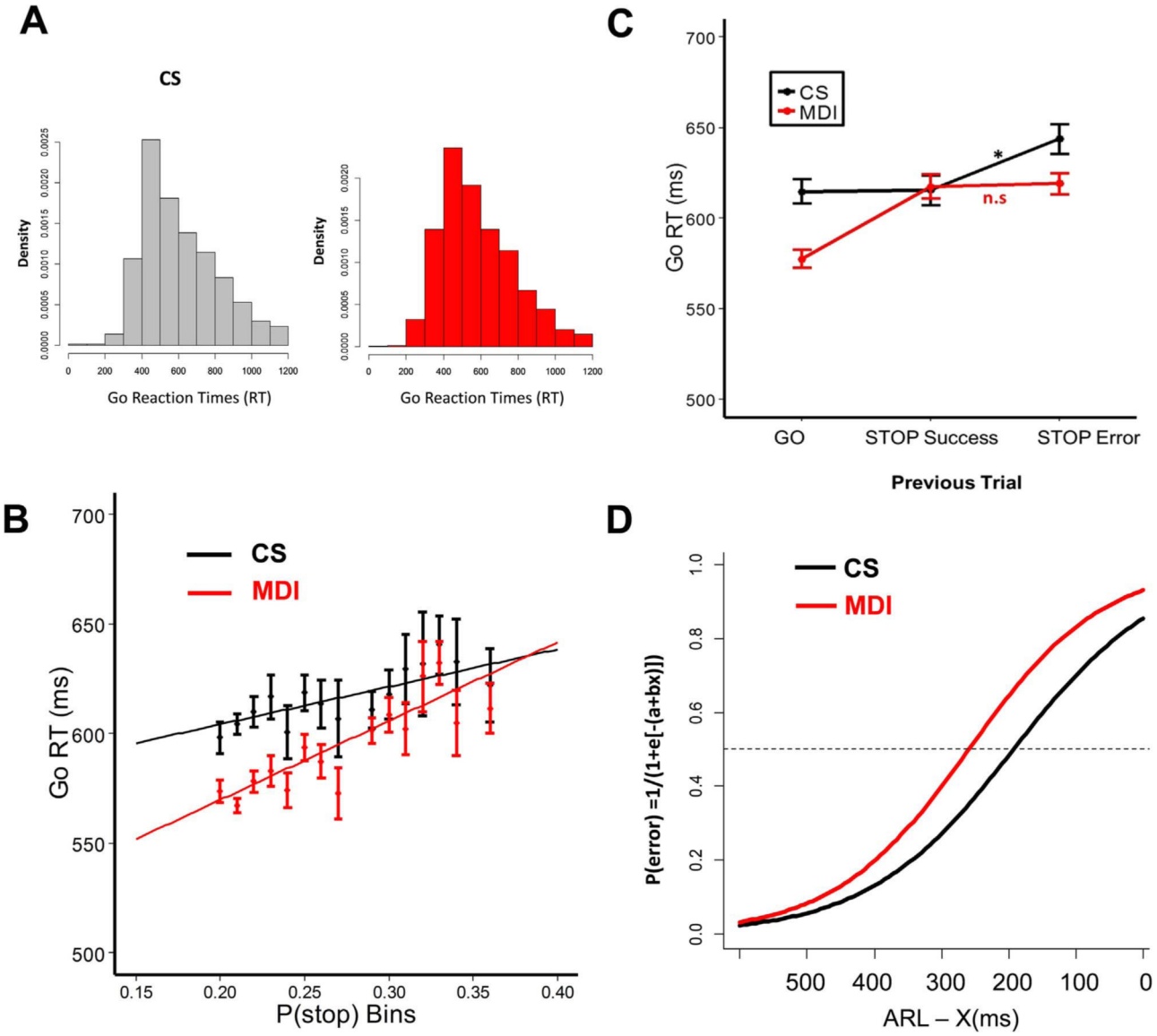

Figure 2.

(A) Histograms of go reaction times (RT) for both control subjects ([CSs]; gray; $n = 36$) and methamphetamine-dependent individuals ([MDIs]; red; $n = 63$) groups. **(B)** Bayesian model prediction and behavioral data presented for each group: red for MDI, black for CS. As predicted by our Bayes optimal decision-making model, a significant positive relationship was observed between individuals' go RT and trialwise P(stop) model estimates in each group. CS (black) and MDI (red) model lines represent best linear regression fit to mean go RT. Error bars are SEM for P(stop) bins. **(C)** Go RTs on trials following a go, successful stop (stop success), or failed stop trial (stop error). CSs had similar RTs following go and successful stop trials, but exhibited slower reaction times following stop error trials ($p < .05$). MDIs were generally slower on stop trials relative to go trials, but they did not exhibit a similar slowing after stop error trials relative to stop success trials ($p > .05$). Error bars are within-group SEM. **(D)** Fitted logistic inhibitory functions by group representing the

likelihood of error on stop trials as a function of the stop signal delay, that is, individual mean go RT (i.e., average response latency [ARL]) – X with X ranging from 500 ms to 0 ms. n.s., not significant.

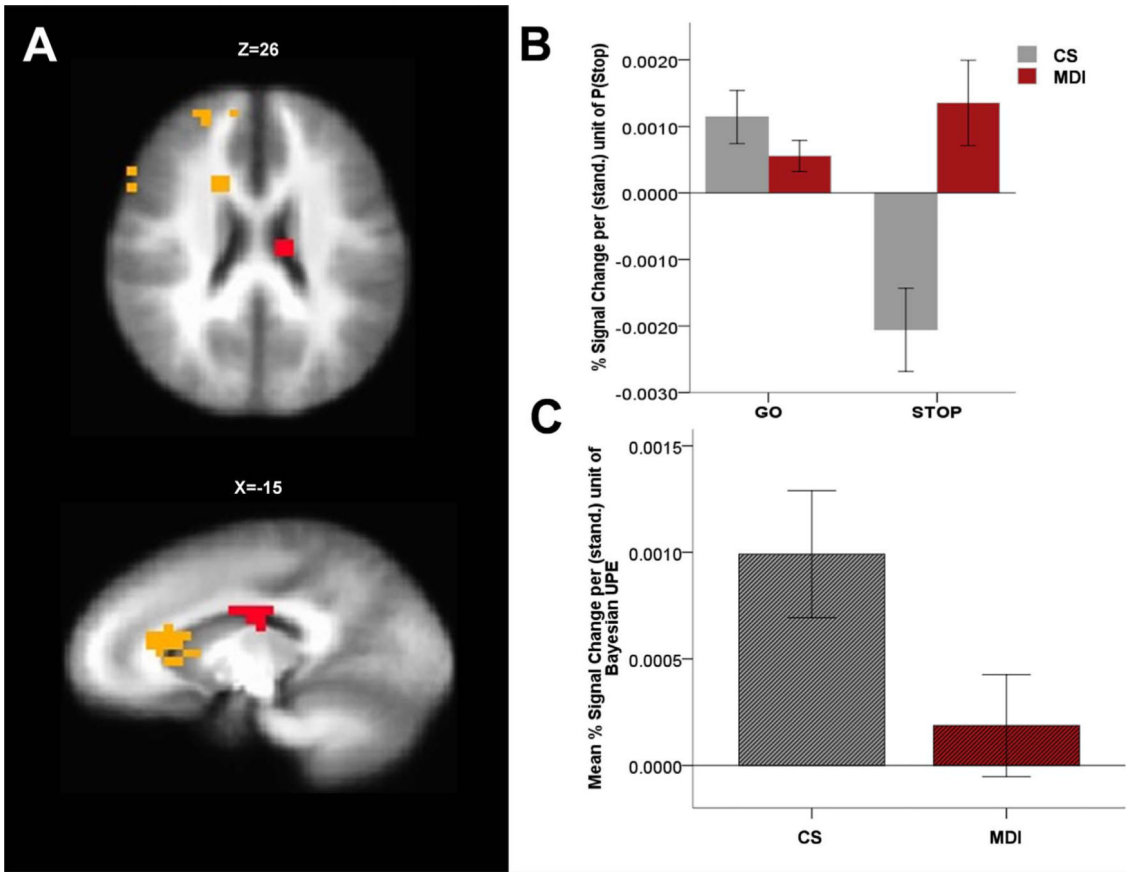

Figure 3.

Group difference in sensitivity to surprising trials, that is, in activation to Bayesian unsigned prediction error (UPE), in the left posterior caudate. **(A)** Blood oxygen level–dependent signal in the posterior caudate showing group difference in percentage signal change modulation by UPE (red cluster). Yellow areas are other regions surviving whole brain analysis for a significant interaction between group and P(stop)-modulated trial type, but in which activation patterns are not consistent with a neural response correlated with a Bayesian UPE or signed prediction error. **(B)** Bar graph displays average P(stop) modulation of percentage signal change by trial type (go vs. stop) and group (control subjects [CSs]: n = 34; methamphetamine-dependent individuals [MDIs]: n = 62; error bars indicate ±1 SEM). In this area, CS (gray bars) demonstrated a neural response consistent with a positive UPE (|outcome - P(stop)|), in other words, a positive correlation between percentage signal change and P(stop) on go trials and a negative correlation on stop trials, whereas MDIs (maroon bars) failed to show such differential P(stop)-dependent activation. **(C)** Average percentage signal change correlation with a positive Bayesian UPE (|outcome - P(stop)|) for each group (error bars: ±1 SEM). Relative to CSs (gray, black stripes), MDIs (maroon, black stripes) showed attenuated UPE-dependent activation (Cohen's d = .45). β was not statistically different from 0 in the MDI group (p > .05).

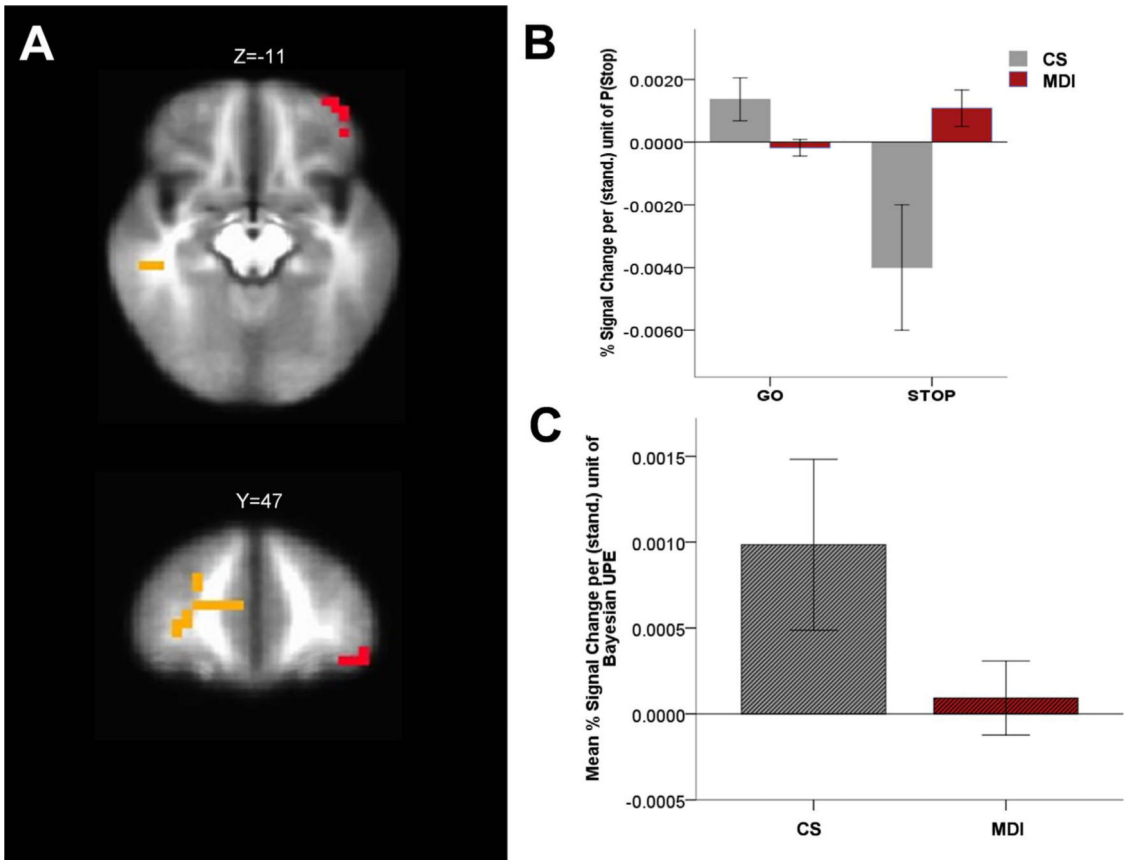

Figure 4.

Group difference in sensitivity to surprising trials, that is, in neural activation to a Bayesian unsigned prediction error (UPE) in the left middle frontal gyrus (Brodmann area 11). **(A)** Blood oxygen level–dependent signal in the left middle frontal gyrus a showing group difference in percentage signal change modulation by UPE (red cluster). Yellow areas are other regions surviving whole brain analysis for a significant interaction between group and P(stop)-modulated trial type, but in which activation patterns are not consistent with a neural response correlated with a Bayesian UPE or signed prediction error. **(B)** Bar graph displays average P(stop) modulation of percentage signal change by trial type (go vs. stop) and group (control subjects [CSs]: $n = 34$; methamphetamine-dependent individuals [MDIs]: $n = 62$; error bars indicate ±1 SEM). In this area, CSs (gray bars) demonstrated a neural response consistent with a positive UPE (|outcome - P(stop)|), in other words, a positive correlation between percentage signal change and P(stop) on go trials and a negative correlation on stop trials, whereas MDIs (maroon bars) failed to show such differential P(stop)-dependent activation. **(C)** Average percentage signal change correlation with a positive Bayesian UPE (|outcome - *P*(stop)|) for each group (error bars: ±1 SEM). Relative to CSs (gray, black stripes), MDIs (maroon, black stripes) showed attenuated UPE-dependent activation (Cohen's $d = .42$). β was not statistically different from 0 in the MDI group ($p > .05$).

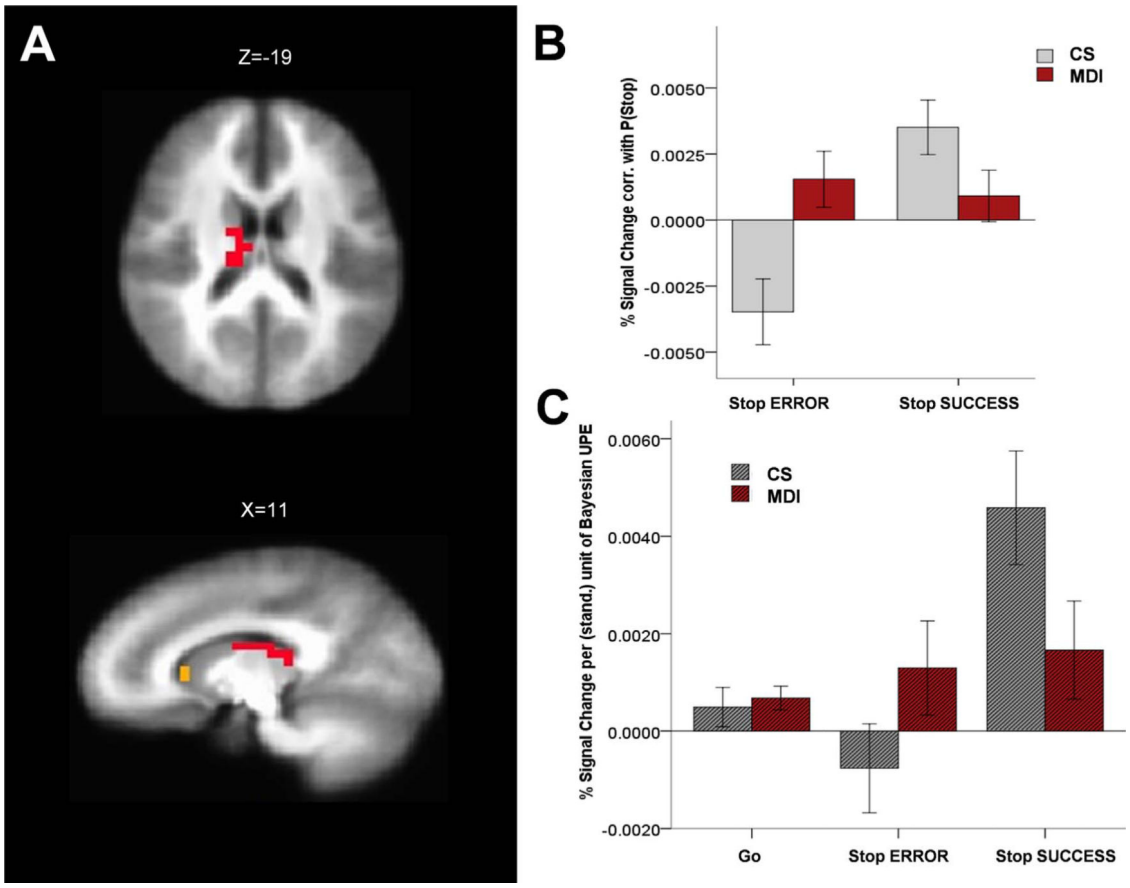

Figure 5.

Group difference in the modulation of neural activation correlated with P(stop) by inhibitory success (right thalamus). **(A)** Blood oxygen level–dependent signal regions representing a significant interaction between group and P(stop)-modulated activation for stop success (SS) vs. stop error (SE) trials (yellow and red clusters). The right thalamus (red cluster), one of these regions, further showed an activation pattern consistent with a group difference in percentage signal change correlated with unsigned prediction error (UPE) on stop error trials. **(B)** Bar graphs represent average percentage signal change for parametric regressors SE × P(stop) and SS × P(stop) in control subjects ([CSs]; $n = 34$) and methamphetamine-dependent individuals ([MDIs]; $n = 62$). Percentage signal change in CSs (gray bars) was negatively correlated with P(stop) on SE trials and positively correlated with P(stop) on SS trials. MDIs (maroon bars) had significantly lower P(stop)-modulated activation on both SS and SE trials, which was not significantly different from 0 ($p > .05$). **(C)** Region of interest analysis (right thalamus). In this region, percentage signal change was selectively positively correlated with a Bayesian UPE, in other words, the amount of surprise or expectancy violation, on SE trials among CSs (gray striped bars), and not significantly correlated with a UPE on successful go and stop trials. In contrast, no statistically significant UPE-dependent activation was observed in MDIs for any type of trial (successful or errors; $p > .05$; group difference on SE: Cohen's $d = .41$); error bars indicate ±1 SEM.

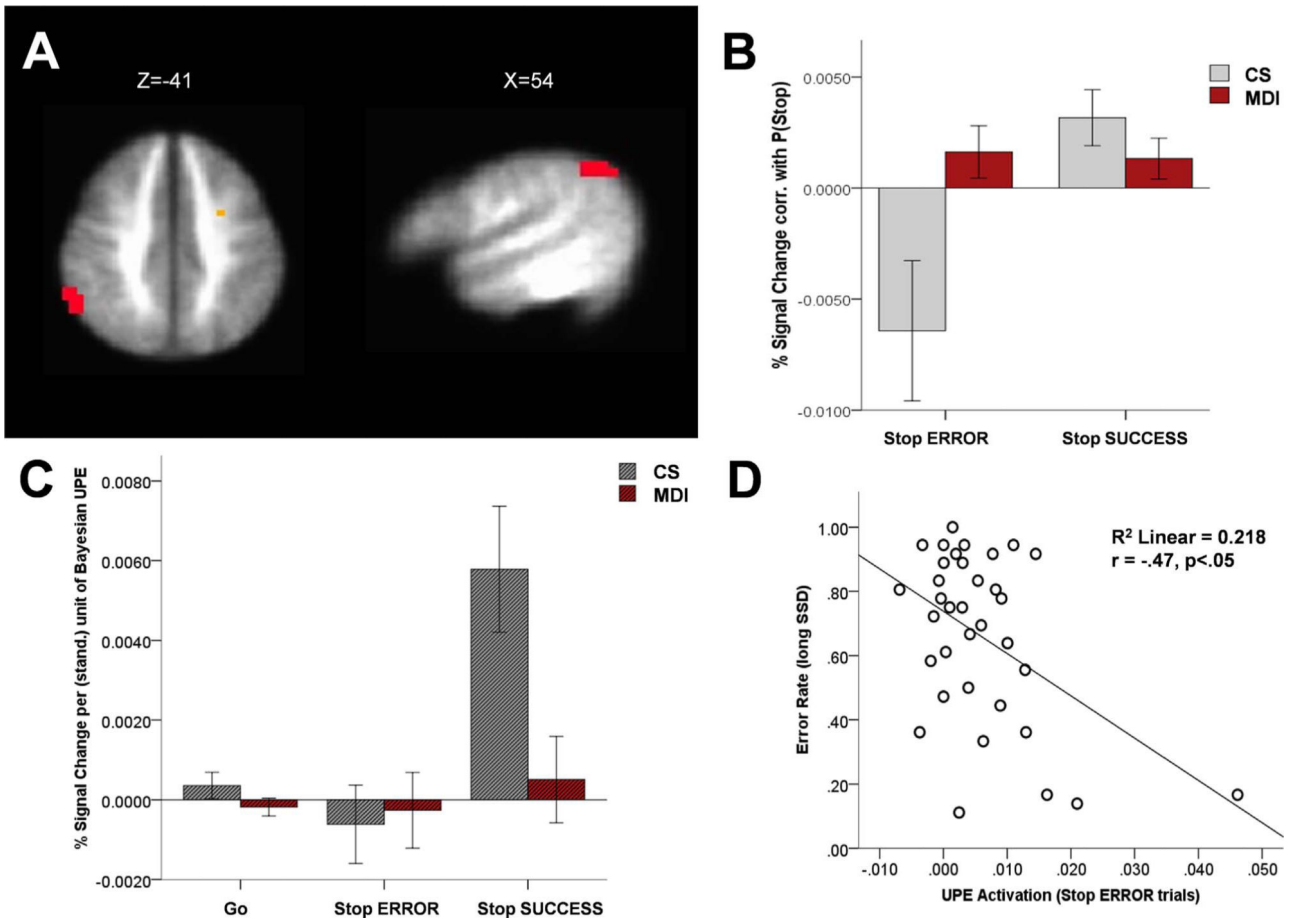

Figure 6.

Group difference in the modulation of neural activation correlated with P(stop) by inhibitory success (right inferior parietal lobule [IPL]; Brodmann area 40). **(A)** Blood oxygen level–dependent signal regions representing a significant interaction between group and P(stop)-modulated activation for stop success (SS) vs. stop error (SE). The IPL (red cluster), one of these regions, further showed an activation pattern consistent with a group difference in percentage signal change correlated with unsigned prediction error (UPE) on SE trials. **(B)** Bar graphs represent average percentage signal change for parametric regressors SE × P(stop) and SS × P(stop) in control subjects ([CSs]; $n = 34$) and methamphetamine-dependent individuals ([MDIs]; $n = 62$). Percentage signal change in CSs (gray bars) was negatively correlated with P(stop) on SE trials and positively correlated with P(stop) on SS trials. MDIs (maroon bars) had significantly lower P(stop)-modulated activation on both SS and SE trials, which was not significantly different from 0 ($p > .05$). **(C)** Region of interest analysis. In this region (right IPL), percentage signal change was selectively positively correlated with a Bayesian UPE, that is, the amount of surprise or expectancy violation, on SE trials among CSs (gray striped bars), and not significantly correlated with a UPE on successful go and stop trials. In contrast, no statistically significant UPE-dependent activation was observed in MDI for any type of trial (successful or errors; $p > .05$); group difference on SE trials: Cohen's $d = .62$; error bars indicate 61 SEM. **(D)** This UPE activation on SE trials in the right IPL among CSs was further associated with lower error

rates on difficult trials (stop signal delays > mean reaction time 200 ms). Graph shows the scatter plot for this significant negative correlation (r = −.47, $p < .05$; we note that a significant correlation was maintained with removal of outlier with high UPE value, i.e., $r = -.36$, $p < .05$; scatter for MDIs not shown because UPE activation was not significantly different from 0).

Table 1

Participants' Characteristics as a Function of Group Status (n = 96)

	Methamphetamine-Dependent Individuals (*n* = 62)		Control Subjects (*n* = 34)		
	Mean	**SD**	**Mean**	**SD**	***t* Test, *p* Value**
Demographics					
Age, years	38.0	10.4	36.1	11.1	.39
Education, years	13.0	1.7	14.8	1.6	<.001
Verbal IQ, WTAR	109.1	8.7	111.6	9.7	.26
Alcohol, typical drinks/week	22.1	38.6	3.9	4.5	<.05
Alcohol, typical days/week	3.1	3.0	1.9	2.2	<.05
Nicotine, typical cigarettes/day	14.0	8.6	1.5	4.0	<.05
Nicotine, typical days/week	6.2	2.2	1.2	2.5	<.05
Lifetime Drug Use					
Methamphetamine	14,267.8	29,028.0	0.0	0.0	N/A
Cocaine	2560.5	6064.4	1.3	4.6	<0.001[a]
Prescription stimulant	56.7	417.5	0.0	0.2	.25[a]
Cannabis	8853.2	25738.0	40.0	168.9	<.001[a]

IQ, intelligence quotient; N/A, not applicable; WTAR, Wechsler Test of Adult Reading.

[a] *t* test computed using natural log transformed + 0.5 values (due to nonnormal distributions) replicated results for raw data.

Table 2

BOLD Activation Foci for Group by P(Stop)-Modulated Trial Type (Go vs. Stop) Interaction

Region	Peak Voxel Talairach Coordinates (*x, y, z*)			Peak Voxel *Z* statistics (*p* Value)	Cluster Size (Voxels)
Right Anterior Cingulate Cortex (BA32)	20	36	12	4.71 (.00001)	215
Left Frontal Caudate	−16	22	11	3.81 (.00014)	53
Right Dorsolateral Prefrontal Cortex (BA 9)	44	17	39	4.21 (.00003)	34
Right Inferior Frontal Gyrus (BA 44)	53	16	18	3.31 (.00093)	17
Left Posterior Caudate	−15	−14	26	3.57 (.00036)	16
Left Orbitofrontal Gyrus (BA 11)	−38	47	−11	3.42 (.00063)	14
Right Middle Temporal Gyrus (BA 22)	51	−33	0	2.90 (.00373)	13

Whole brain random effect analysis; corrected for clusterwise significance: $p < .01$; minimum voxel significance is $p < .005$ and minimum cluster size is 12 voxels/768 μL).

BA, Brodmann area; BOLD, blood oxygen–level dependent.

Table 3

BOLD Activation Foci for Group by P(Stop)-Modulated Stop Trial Type (SS vs. SE) Interaction

Region	Peak Voxel Talairach Coordinates (*x, y, z*)			Peak Voxel *Z* statistics (*p* Value)	Cluster Size (Voxels)
Left Precentral Gyrus	−26	4	33	3.71 (.00021)	19
Right Caudate (BA 25)	3	19	5	3.18 (.00147)	15
Right Thalamus	11	−18	19	2.99 (.00279)	14
Left Postcentral Gyrus (BA 2)	−54	−18	32	3.25 (.00115)	13
Left Inferior Semilunar Lobule	−18	−77	−36	3.74 (.00018)	12
Right Inferior Parietal Lobule (BA 40)	54	−51	41	3.39 (.00070)	12

Whole brain random effect analysis; corrected for clusterwise significance: $p < .01$; minimum voxel significance is $p < .005$ and minimum cluster size is 12 voxels/768 μL).

BA, Brodmann area; BOLD, blood oxygen level dependent; SE, stop error; SS, stop success.